Journal of Materials Science: Materials in Electronics (2018) 29:17552–17562
https://doi.org/10.1007/s10854-018-9857-7

CTAB-assisted microemulsion synthesis of unique 3D network nanostructured polypyrrole presenting significantly diverse capacitance performances in different electrolytes

Caixia Li[1] · Ping He[1,2] · Zhen Tang[1] · Mingqian He[3] · Faqin Dong[4] · Xiaojuan Zhang[1] · Huanhuan Liu[1] · Shuai Wang[1]

Received: 22 March 2018 / Accepted: 9 August 2018 / Published online: 12 August 2018

Abstract

In this work, the unique 3D network nanostructured polypyrrole (PPy) has been successfully synthesized in cetyltrimethylammonium bromide/butyl alcohol/hexane/water microemulsion system. The composition, crystalline characteristic and morphology of as-prepared PPy materials are characterized by Fourier transform infrared spectrometer, X-ray diffractometer and field emission scanning electron microscope. It is shown that as-prepared PPy materials possess unique 3D network nanostructure stacked by PPy nanospheres with an average diameter of 100 nm. Furthermore, the electrochemical performances of PPy based electrodes are investigated by cyclic voltammetry, galvanostatic charge/discharge and electrochemical impedance spectrum in 1.0 M H_2SO_4, 1.0 M Na_2SO_4 and 1.0 M KCl electrolytes, respectively. At a current density of 1.0 A g^{-1}, as-prepared PPy based electrode exhibits the highest specific capacitance (329.0 F g^{-1}) in 1.0 M H_2SO_4 electrolyte, much higher than that in 1.0 M Na_2SO_4 (156.6 F g^{-1}) or 1.0 M KCl (153.2 F g^{-1}) electrolyte. However, the specific capacitance of PPy based electrode in 1.0 M H_2SO_4 electrolyte retains only 40.6% of the initial specific capacitance after 5000 continuous charge/discharge cycles and, interestingly, 83.9% and 81.3% in 1.0 M Na_2SO_4 and 1.0 M KCl electrolytes, respectively. It is reasonable that the process of deoxidation and reoxidation of PPy nanomaterials is accompanied by the intercalation and deintercalation of massive H_3O^+ in 1.0 M H_2SO_4 electrolyte, which might result in the collapsed structure of as-prepared PPy nanomaterials and the relative instability during the cycling process.

1 Introduction

Nowadays, the demands for sustainable and clean energy are becoming more and more critical owing to the increasing environmental problems, such as the shortage of resource, pollution and global warming. Hence, it is realistically significant to develop new, low-cost and eco-friendly energy conversion and storage system [1, 2]. As a new type of energy storage devices, supercapacitors have attracted significant attentions due to high power density and exceptionally long cycle life, etc [3–5]. In general, according to the charge storage mechanism, supercapacitors can be classified into two types, including electrochemical double layer capacitors and pseudocapacitors [6–8]. It is well known that the key factor to develop high-performance supercapacitors is the design and synthesis of electrode materials with excellent electrochemical properties and high conductivity [9]. Generally, three kinds of electrode materials have been used for the fabrication of supercapacitors, including carbon based materials (activated carbon, carbon nanotubes and graphene, etc.) [10–12], metal compound (metal oxide, metal hydroxide

✉ Ping He
heping@swust.edu.cn

✉ Faqin Dong
fqdong@swust.edu.cn

1 State Key Laboratory of Environment-Friendly Energy Materials, School of Materials Science and Engineering, Southwest University of Science and Technology, Mianyang 621010, People's Republic of China

2 Mianyang Kingtiger New Energy Technology Co. Ltd., Mianyang 621010, People's Republic of China

3 Sichuan Changhong New Energy Technology Co. Ltd., Mianyang 621010, People's Republic of China

4 Key Laboratory of Solid Waste Treatment and Resource Recycle of Ministry of Education, Southwest University of Science and Technology, Mianyang 621010, People's Republic of China

and metal sulfide, etc.) [13–15] and conducting polymers (polypyrrole, polyaniline and polythiophene, etc.) [16–18].

Among electrode materials above, conducting polymers play a vital role in high-performance supercapacitors owing to their advantages of high conductivity and redox properties, etc [19, 20]. As one kind of conducting polymers, polypyrrole (PPy) has attracted much attention due to its wide potential window, high conductivity, high capacitance and low cost, etc [21, 22]. Up to now, PPy has been widely used in electrochemical fields, such as sensors, corrosion protection, secondary batteries and supercapacitors [23–26].

To improve the electrochemical performance of supercapacitors, the growing interest has concentrated on controlling microstructures of electrode materials via different synthetic routes [27]. In general, PPy nanoparticles or thin films can be fabricated through chemical polymerization or electropolymerization method [28, 29]. However, the traditional chemical polymerization and electropolymerization of conductive polymer materials are easily affected by polymerization rate, solvent nature and media pH, etc [30, 31]. Recently, microemulsion method has received considerable attention for the preparation of nanomaterials [32, 33], where micro/nano droplets of water phase containing reactants are dispersed and stabilized by a surfactant in an organic medium, resulting in morphologically controllable nanomaterials. Therefore, the nanomaterials with different sizes can be prepared by altering different components involved in the formation of surfactant-assisted microemulsion [34].

In addition, electrolyte is another important factor in influencing the performance of supercapacitors [35]. Electrolytes used in supercapacitors can be classified into three categories, including aqueous, organic and ionic liquids based electrolytes. In general, aqueous based electrolytes have attracted more attention due to their higher concentration and smaller ionic radius, which can provide higher conductivity than organic based electrolytes [36]. Among the aqueous based electrolytes, H_2SO_4, Na_2SO_4 and KCl are frequently employed as electrolytes in supercapacitors because of their desired properties, such as high conductivity, low viscosity and low cost, etc [35]. Unfortunately, most of researches focus on the electrode materials although the selection of electrolyte is an important factor in affecting the electrochemical performance of supercapacitors [37]. Based on the consideration above, H_2SO_4, Na_2SO_4 and KCl are chosen as electrolytes to investigate the electrochemical behavior of as-prepared PPy nanomaterials fabricated by microemulsion method.

In this work, the unique 3D network nanostructured PPy built by nanospheres was successfully synthesized via a simple and effective CTAB-assisted microemulsion method and the electrochemical performances of as-prepared PPy based electrodes were assessed in 1.0 M H_2SO_4, 1.0 M Na_2SO_4 and 1.0 M KCl electrolytes, respectively. As-prepared PPy based electrode exhibited the highest specific capacitance in 1.0 M H_2SO_4 electrolyte, but the capacitance retention of as-prepared PPy based electrode in 1.0 M H_2SO_4 electrolyte was lower than that in 1.0 M Na_2SO_4 or 1.0 M KCl electrolyte after 5000 continuous charge/discharge cycles.

2 Experimental

2.1 Reagents and materials

Ammonium persulfate (APS), cetyltrimethylammonium bromide (CTAB), *n*-butyl alcohol, *n*-hexane, ethanol, H_2SO_4, Na_2SO_4 and KCl were analytically pure grade and purchased from Aldrich Chemical Reagent Co. Ltd. (Chengdu, China). Conductive carbon black and polytetrafluoroethylene (PTFE) were obtained from Tianjin Chenhua Chemical Reagent Factory (Tianjin, China).

Pyrrole monomer (Py) was purchased from Chengdu Institute of Organic Chemistry, Chinese Academy of Science (Chengdu, China). Py was purified through distillation under reduced pressure and stored at a temperature of less than 5 °C before use.

Ni foam was purchased from Jinan Henghua Chemical Reagent Factory (Jinan, China). Ni foam substrates were pre-treated under ultrasonication by sequentially immersing in acetone, distilled water and ethanol each for 20 min and dried at 60 °C for 24 h before use. Distilled water was used throughout the whole experiments.

2.2 Synthesis of PPy materials

The preparation of PPy was described as follows. Firstly, 1.14 g APS was dissolved into 10 mL distilled water and stirred with a magnetic stirrer. Secondly, 0.040 g CTAB, 0.90 mL *n*-butyl alcohol and 6.0 mL *n*-hexane were slowly added into the solution above. Then, the mixed solution above was put into ice bath at a temperature of 0 °C under stirring to form a transparent microemulsion system. Next, 5.0 mmol Py (350 μL) was slowly injected into the microemulsion system, and some black flocculent products appeared at organic/aqueous interface. After stirring for 12 h in ice bath, the product was obtained by demulsification with ethanol, washed with ethanol and distilled water for several times and dried at 70 °C for 24 h in air.

2.3 Characterization of as-prepared PPy materials

Fourier transform infrared (FTIR) spectroscopy of as-prepared PPy materials was acquired by Nicolet-5700 (Nicolet Instrument Co., America) in the wavenumber range of 4000–500 cm^{-1}. The crystal structure of as-prepared PPy

materials was determined by X'Pert PRO (XRD, PANalytical B.V., Holland) using Cu K_α radiation ($\lambda = 0.154060$ nm) recorded from 5° to 70° at a speed of 2° min^{-1}. The morphology and microstructure of as-prepared PPy materials were investigated by Ultra 55 microscope (FE-SEM, Carl Zeiss SMT Pte Ltd, Germany).

2.4 Preparation of PPy based electrode

As-prepared PPy based electrode was fabricated as follows. Briefly, as-prepared PPy nanomaterials, conductive carbon black and 10% PTFE emulsion were mixed with a mass ratio of 8:1:1 and dispersed in ethanol. The mixture was ultrasonically treated for 10 min and placed in an oven at 60 °C to form sticky slurry. Then, the resulting sticky slurry was pasted onto Ni foam with size of 1.0 cm × 2.0 cm (coated active area = 1.0 cm^2), followed by drying at 60 °C under vacuum for 12 h. Finally, the coated Ni foam was pressed to a thin foil under a pressure of 5.0 MPa.

2.5 Electrochemical measurements

Electrochemical tests of cyclic voltammetry (CV), galvanostatic charge/discharge (GCD) and electrochemical impedance spectrum (EIS) were conducted with an electrochemical workstation (PARSTAT 2273, Ametek, USA) in 1.0 M H_2SO_4, 1.0 M Na_2SO_4 and 1.0 M KCl electrolytes, respectively. A three-electrode system consisted of platinum electrode as counter electrode, as-prepared PPy based electrode as working electrode and saturated calomel electrode (SCE) as reference electrode. CV and GCD measurements were conducted in the potential range of − 0.2 to 0.8 V in 1.0 M H_2SO_4 electrolyte or − 0.5 to 0.5 V in both 1.0 M Na_2SO_4 and 1.0 M KCl electrolytes. EIS measurements were performed in the frequency range of 10^5–10^{-1} Hz at open-circuit potential with an ac-perturbation of 5 mV.

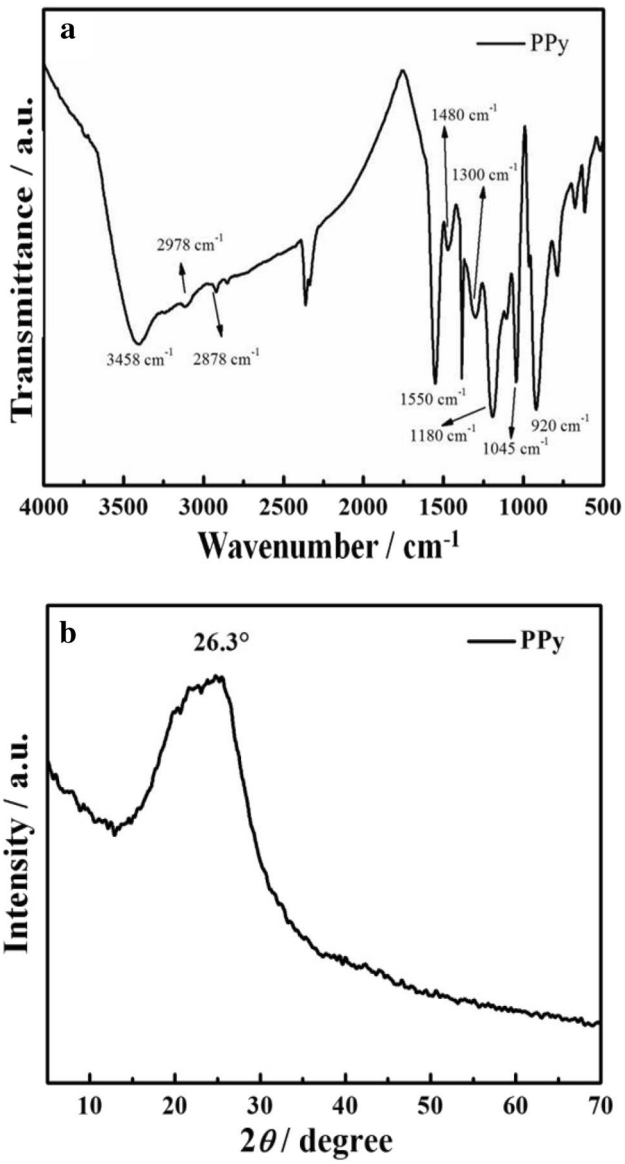

Fig. 1 FTIR spectrum (**a**) and XRD pattern (**b**) of as-prepared PPy materials

3 Results and discussion

3.1 FTIR and XRD analyses of as-prepared PPy materials

Shown in Fig. 1a was FTIR spectrum of as-prepared PPy materials. The broad band was observed at 3500 to 3000 cm^{-1}, corresponding to the stretching vibration of C–H and N–H of pyrrole ring [38]. The fundamental vibrations of Py ring located at 1550 cm^{-1} and 1480 cm^{-1} were ascribed to the antisymmetric and the symmetric ring-stretching modes, respectively [39]. The absorption bands at 1300 cm^{-1} and 1180 cm^{-1} were attributed to the in-plane deformation of =C–H, and the out-of-plane vibration of =C–H at 920 cm^{-1} was also observed [40]. The absorption band at 1405 cm^{-1} was due to the stretching vibration of C–N [38]. These results above confirmed that as-prepared materials were pure polypyrrole.

XRD spectrum of as-prepared PPy materials was presented in Fig. 1b. It was observed that a broad diffraction peak was located at 2θ angle around 26.3°, indicating that as-prepared PPy was a kind of amorphous materials with low crystallinity which could facilitate the penetration of ions through the bulk of active materials [41, 42].

3.2 SEM analysis of as-prepared PPy nanomaterials

Shown in Fig. 2 were SEM images of as-prepared PPy nanomaterials under different magnifications. It was observed that as-prepared PPy materials exhibited a unique 3D network nanostructure stacked by a large number of nanospheres with an average diameter around 100 nm, and the surface of PPy nanospheres possessed open channeled structure, resulting in large specific surface area. The unique 3D network nanostructure of PPy materials could provide abundant active sites for electrochemical reactions and be beneficial to the diffusion of ions, resulting in enhanced electrochemical performance [43].

3.3 Electrochemical performances of as-prepared PPy based electrode

Shown in Fig. 3a, b, c were the typical CVs of as-prepared PPy based electrodes at different scan rates in 1.0 M H_2SO_4, 1.0 M Na_2SO_4 and 1.0 M KCl electrolytes, respectively. It was observed that the CVs of as-prepared PPy based electrodes had no obvious redox peak in 1.0 M H_2SO_4, 1.0 M Na_2SO_4 and 1.0 M KCl electrolytes. It was reported that the CVs of PPy based electrode with pseudocapacitance behavior exhibited nearly rectangular shape [44]. As shown in Fig. 3a, b, c, the CV curves of PPy based electrodes were similar and presented nearly rectangular shape in three electrolytes, indicating that PPy based electrode exhibited pseudocapacitance behavior. The results above were consistent with the reported literatures [45, 46].

In addition, the CVs of as-prepared PPy based electrode deviated slightly from the rectangular shape in 1.0 M H_2SO_4 electrolyte at higher scan rates (Fig. 3a). In contrast, the CV curves of PPy based electrodes exhibited similar shapes at different scan rates in 1.0 M Na_2SO_4 and 1.0 M KCl electrolytes (Fig. 3b, c), indicating a high rate-capability and efficient ionic and electronic transport in Na_2SO_4 and KCl electrolytes [46].

Shown in Fig. 3d was the comparison of CVs of as-prepared PPy based electrodes in three electrolytes at a scan rate of 5 mV s^{-1}. It was observed that the integral area of CV in 1.0 M H_2SO_4 electrolyte was larger than that in 1.0 M Na_2SO_4 or 1.0 M KCl electrolyte, suggesting that as-prepared PPy based electrode exhibited the highest specific capacitance in H_2SO_4 electrolyte.

Shown in Fig. 4a were GCDs of as-prepared PPy based electrode at different current densities in 1.0 M H_2SO_4 electrolyte. It was observed that a smaller potential platform appeared at the GCDs of as-prepared PPy based electrode in 1.0 M H_2SO_4 electrolyte due to the intercalation and deintercalation of massive H_3O^+ [47]. In contrast, the GCDs of as-prepared PPy based electrodes were regular symmetrical triangles in 1.0 M Na_2SO_4 and 1.0 M KCl electrolytes

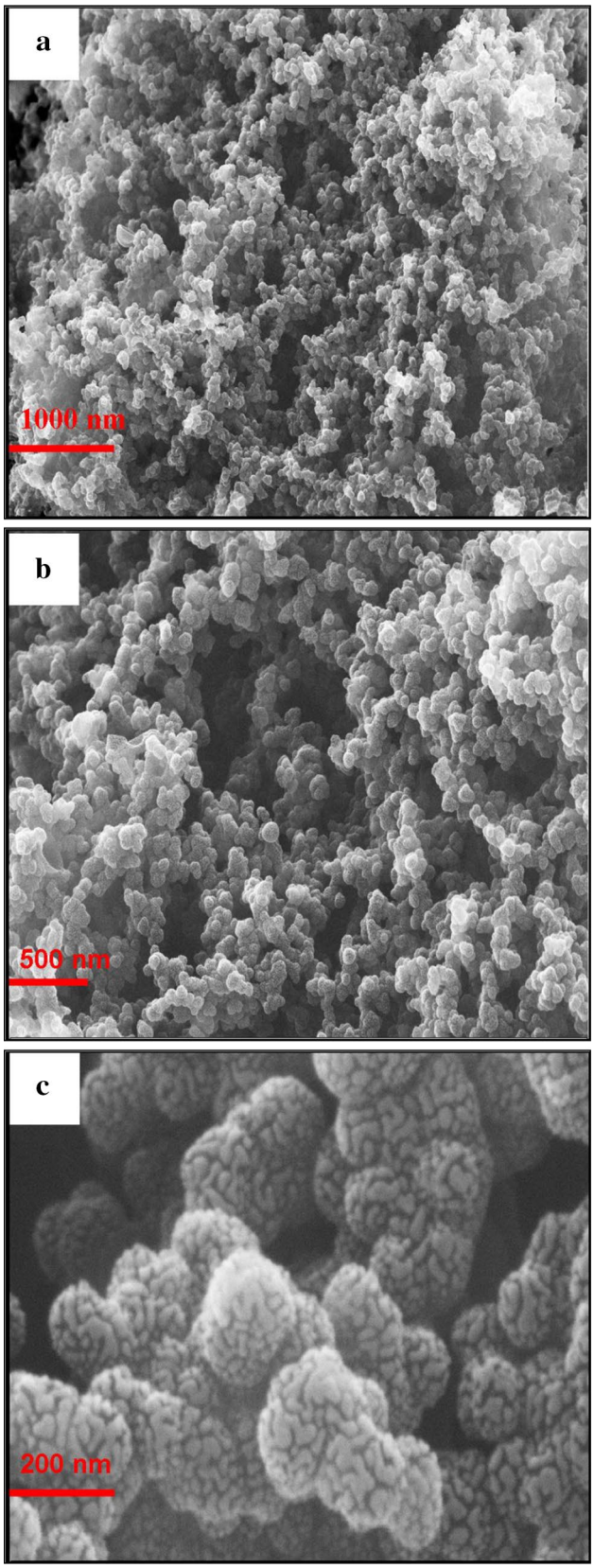

Fig. 2 SEM images of as-prepared PPy nanomaterials under different magnifications

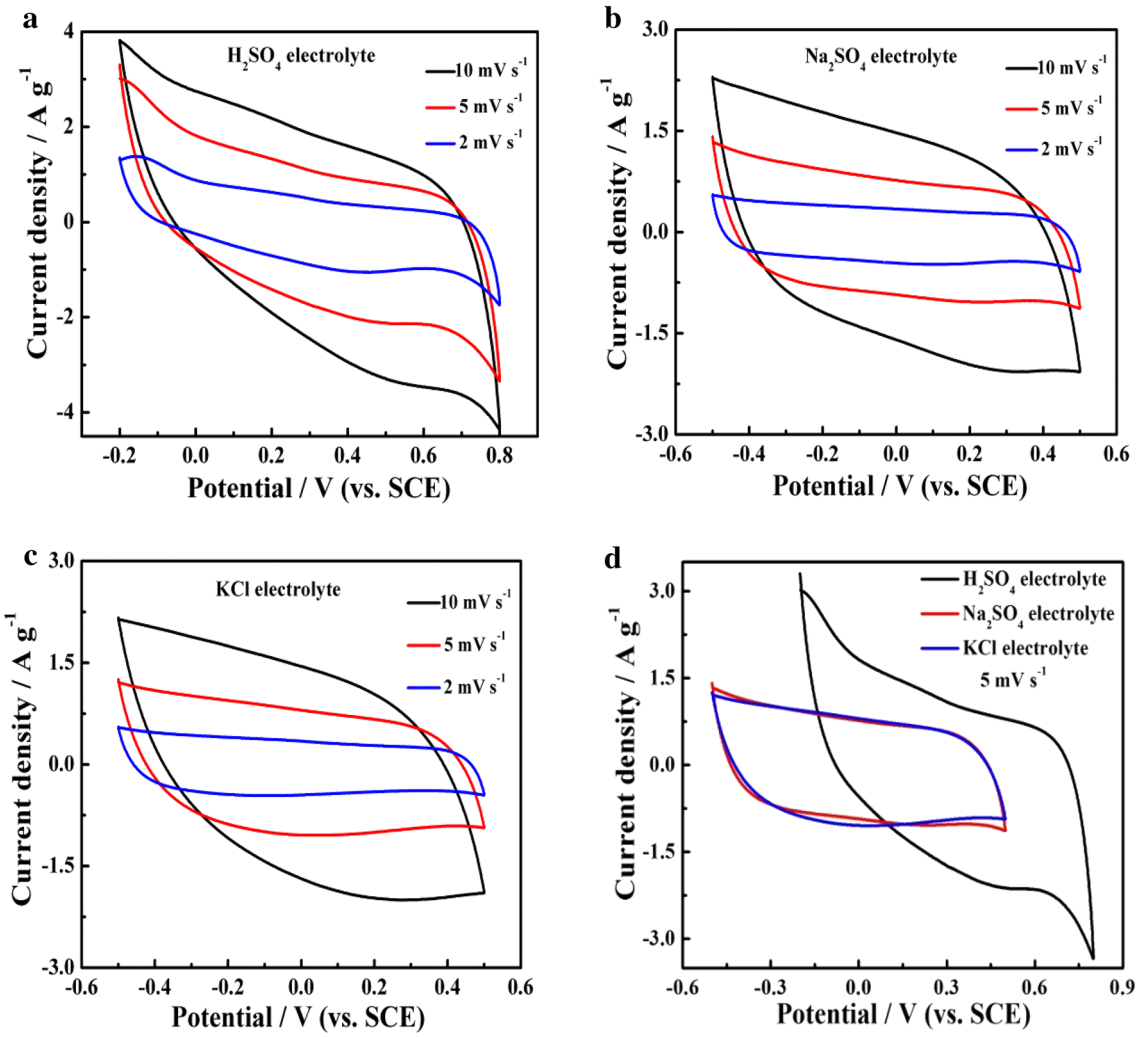

Fig. 3 CVs of as-prepared PPy based electrodes in 1.0 M H_2SO_4 (**a**), 1.0 M Na_2SO_4 (**b**) and 1.0 M KCl (**c**) electrolytes at different scan rates, and comparison of CVs in three electrolytes at a scan rate of 5 mV s^{-1} (**d**)

at different current densities (Fig. 4b, c), and the potential of electrode showed a favourable linear relationship with increasing time.

The specific capacitances were calculated from the slope of charge/discharge curves according to the equation as follows:

$$C_s = (i \times \Delta t)/(m \times \Delta V) \quad (1)$$

where C_s was the specific capacitance (F g^{-1}), i the discharge current (A), Δt the discharge time (s), m the mass of active materials on Ni foam (g) and ΔV the discharge potential window after the *IR* drop (V) [48].

The calculated specific capacitances of as-prepared PPy based electrodes in 1.0 M H_2SO_4, 1.0 M Na_2SO_4 and 1.0 M KCl electrolytes were 329.0 F g^{-1}, 156.6 F g^{-1} and 153.2 F g^{-1} at a current density of 1.0 A g^{-1} and 331.0 F g^{-1}, 176.2 F g^{-1} and 179.4 F g^{-1}, respectively, at a current density of 0.5 A g^{-1}. Clearly, the specific capacitance of as-prepared PPy based electrode in 1.0 M H_2SO_4 electrolyte was higher than that in 1.0 M Na_2SO_4 or 1.0 M KCl electrolyte at the same current density.

In general, in the process of deoxidation and reoxidation, the electrochemical performance of PPy based electrode was influenced by the intercalation and deintercalation of cations and anions in different electrolytes [43]. And the process of intercalation and deintercalation of ions was closely related to the sizes, radii and conductivities of ions [49]. Listed in Table 1 were the radii and molar ionic conductivities of ions in aqueous solutions [50]. It was shown that H_3O^+ had the smallest ionic radius and highest ionic conductivity. Therefore, the process of deoxidation and reoxidation of PPy nanomaterials was accompanied by the intercalation and deintercalation of massive H_3O^+ in 1.0 M H_2SO_4 electrolyte, resulting in the highest specific capacitance [44].

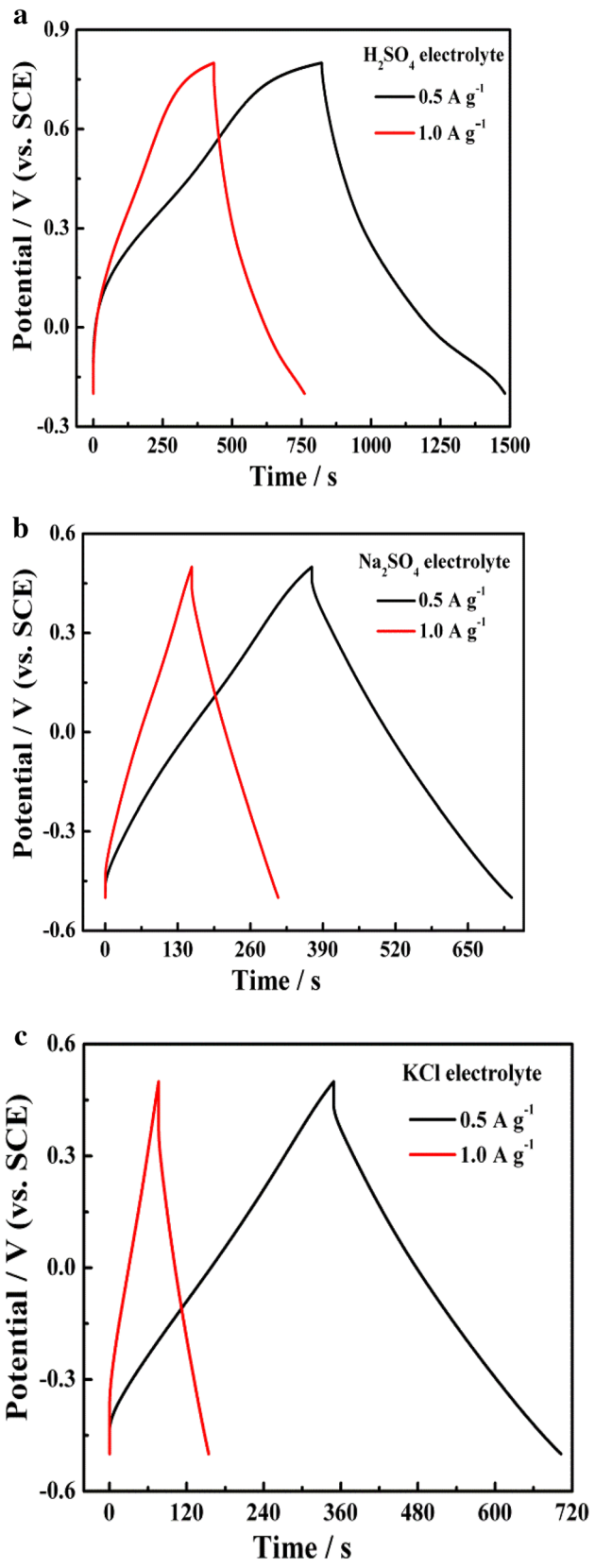

Fig. 4 GCDs of as-prepared PPy based electrodes in 1.0 M H_2SO_4 (**a**), 1.0 M Na_2SO_4 (**b**) and 1.0 M KCl (**c**) electrolytes at different current densities

Table 1 Radii and molar ionic conductivities of ions in aqueous solutions [50]

Ion	Non-hydrated ionic radii (Å)	Hydrated ionic radii (Å)	Ionic conductivity (S cm^2 mol^{-1})
H^+	< 0.50	–	349.8
H_3O^+	1.50	2.82	
Na^+	0.95	3.58	50.1
K^+	1.33	3.31	73.5
Cl^-	1.81	3.32	76.3
SO_4^{2-}	2.58	3.79	160.0
OH^-	1.33	3.00	198.3

The data in Table 1 is derived from the 50th reference in the manuscript

In addition, the calculated specific capacitance of PPy based electrode decreased with increasing current density in 1.0 M H_2SO_4, 1.0 M Na_2SO_4 and 1.0 M KCl electrolytes. It was reasonable that, with increasing current density, concentration polarization increased inevitably. Furthermore, while maintaining high current density necessarily demanded higher excitation voltage, but the numbers of interface charges didn't increase, which would lead to the decrease of specific capacitance [40]. Therefore, the specific capacitance decreased with increasing current density.

Shown in Fig. 5 were cyclic stabilities of as-prepared PPy electrodes at a current density of 1.0 A g^{-1} in 1.0 M H_2SO_4, 1.0 M Na_2SO_4 and 1.0 M KCl electrolytes after 5000 continuous charge/discharge cycles. Illustrated in the inset of

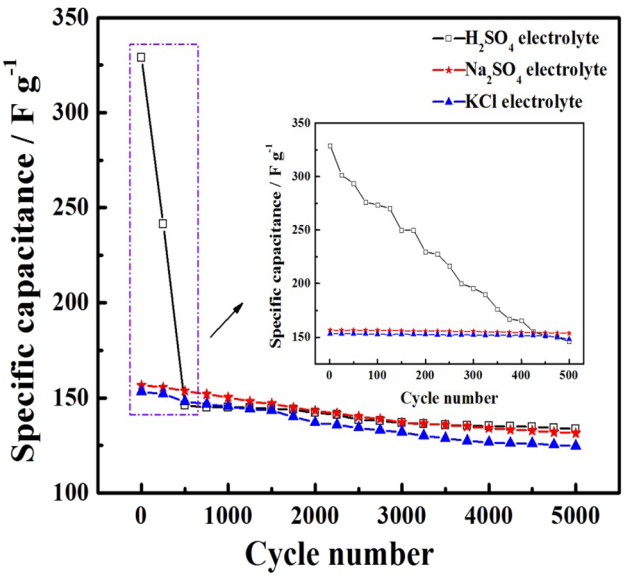

Fig. 5 Cyclic stabilities of as-prepared PPy based electrodes at a current density of 1.0 A g^{-1} in 1.0 M H_2SO_4, 1.0 M Na_2SO_4 and 1.0 M KCl electrolytes. Inset was cyclic stabilities of PPy based electrodes after 500 continuous charge/discharge cycles in three electrolytes

Fig. 5 were cyclic stabilities of PPy based electrodes after 500 continuous charge/discharge cycles in three electrolytes. It was observed that the specific capacitance of as-prepared PPy based electrode in H_2SO_4 electrolyte decayed quickly with increasing cycle number and remained nearly stable after 425 continuous charge/discharge cycles. Moreover, the specific capacitance of as-prepared PPy based electrode in 1.0 M H_2SO_4 electrolyte was similar to those in 1.0 M Na_2SO_4 and 1.0 M KCl electrolytes after 425 continuous charge/discharge cycles.

In addition, after 5000 continuous charge/discharge cycles, the specific capacitance of PPy based electrode in 1.0 M H_2SO_4 electrolyte decayed from 329 to 133.6 F g^{-1}, and the capacitance retention was only 40.6%. In contrast, as-prepared PPy based electrode exhibited higher capacitance retention, 83.9% in 1.0 M Na_2SO_4 and 81.3% in 1.0 M KCl electrolytes, at a current density of 1.0 A g^{-1} after 5000 continuous charge/discharge cycles. The results indicated that the cyclic stability of as-prepared PPy based electrode in 1.0 M H_2SO_4 electrolyte was poorer than that in 1.0 M Na_2SO_4 or 1.0 M KCl electrolyte.

We have further explored the reasons why as-prepared PPy nanomaterials exhibited distinctly different cyclic stabilities in 1.0 M H_2SO_4, 1.0 M Na_2SO_4 and 1.0 M KCl electrolytes. The CVs of as-prepared PPy based electrodes before and after 5000 continuous charge/discharge cycles were measured in three electrolytes at a scan rate of 5 mV s^{-1}. After 5000 continuous charge/discharge cycles, it was shown that the shape of CV curve in H_2SO_4 electrolyte changed and the surrounded area of CV curve decreased to a certain extent (Fig. 6a). In contrast, the shape and integral area of CV curves before and after 5000 continuous charge/discharge cycles had no obvious change in Na_2SO_4 and KCl electrolytes (Fig. 6b, c).

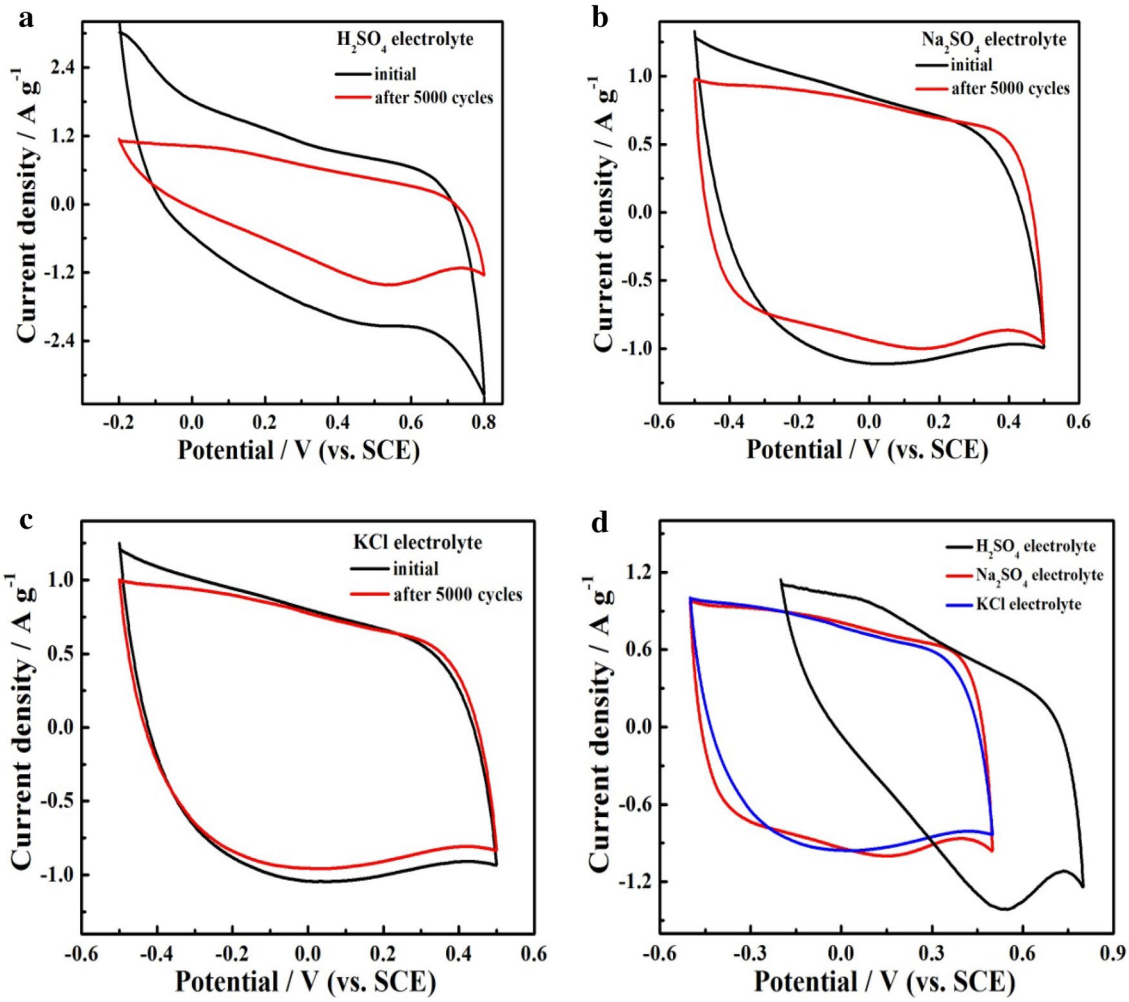

Fig. 6 CVs of as-prepared PPy based electrodes before and after 5000 continuous charge/discharge cycles in 1.0 M H_2SO_4 (**a**), 1.0 M Na_2SO_4 (**b**) and 1.0 M KCl (**c**) electrolytes, and comparison of CVs of as-prepared PPy based electrodes after 5000 continuous charge/discharge cycles in three electrolytes (**d**). Scan rate: 5 mV s^{-1}

The reason for the poor cyclic stability of as-prepared PPy based electrode in H_2SO_4 electrolyte can be interpreted as follows. On the one hand, the process of deoxidation and reoxidation occurred in 3D network nanostructured PPy based electrodes during the cycling process, which might result in the expansion or contraction of crystal microstructure of as-prepared PPy nanomaterials [51]. On the other hand, the process of deoxidation and reoxidation of PPy was accompanied by the intercalation and deintercalation of H_3O^+ due to its smaller ionic radius and higher ionic conductivity [40]. H_2SO_4 solution has a high concentration of H_3O^+, which might easily diffuse into PPy matrix to compensate charge, resulting in high acidity to weaken the activity and damage the nanostructure [52]. Therefore, the collapse of crystal structures or microspheres of as-prepared PPy nanomaterials during the earlier stage of cycling process might result in the relative instability in 1.0 M H_2SO_4 electrolyte.

In order to observe change of the morphology of PPy nanomaterials during the cycling process, SEM measurements were conducted on as-prepared PPy based electrodes after 500, 2500 and 5000 continuous charge/discharge cycles in 1.0 M H_2SO_4, 1.0 M Na_2SO_4 and 1.0 M KCl electrolytes, respectively (Fig. 7). It was observed that the unique 3D network nanostructure of PPy based electrode collapsed seriously in 1.0 M H_2SO_4 electrolyte after 500 continuous charge/discharge cycles (Fig. 7a_1). After 2500 (Fig. 7a_2) and 5000 (Fig. 7a_3) cycles, the collapsed

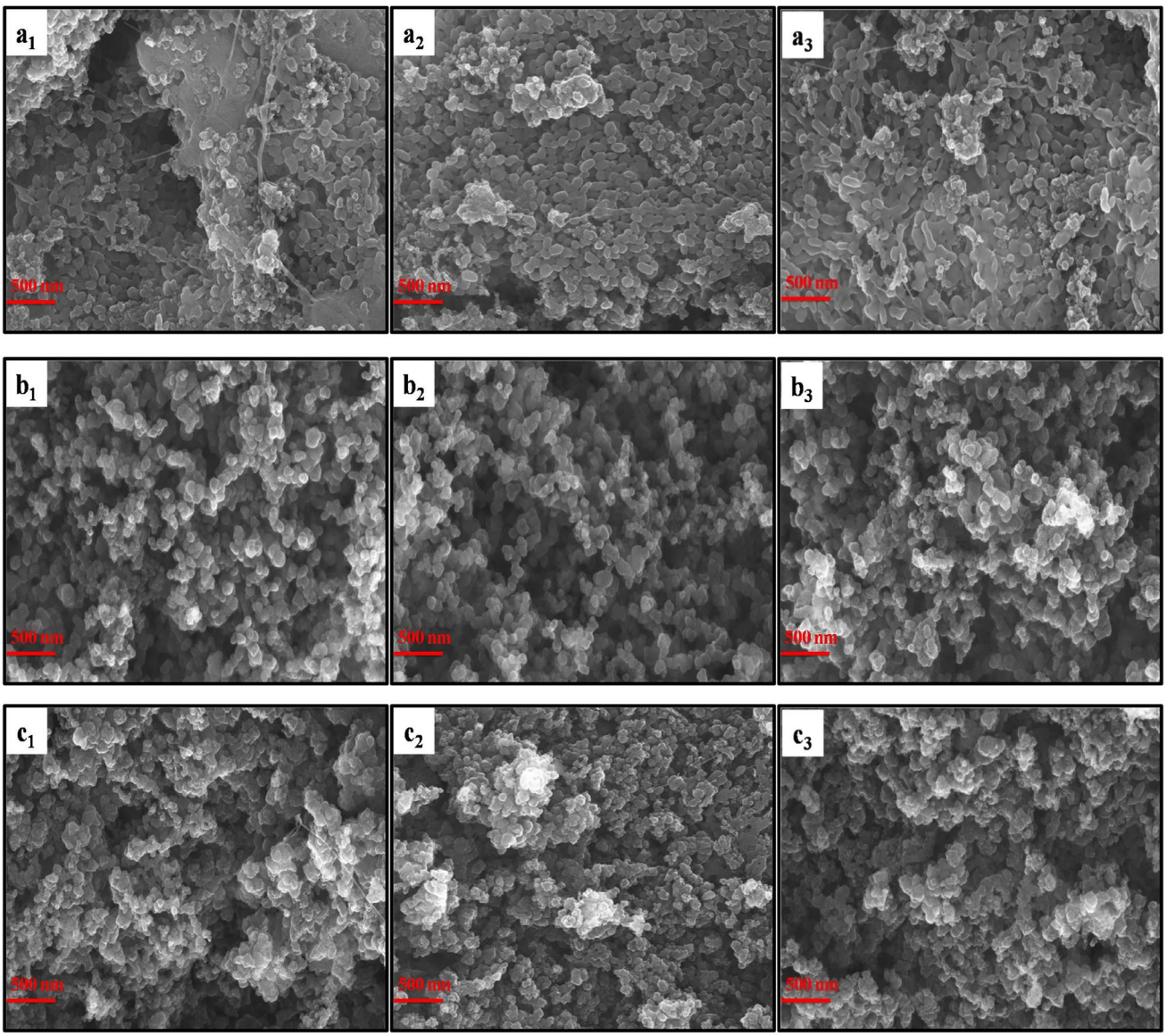

Fig. 7 SEM images of as-prepared PPy based electrodes after 500, 2500 and 5000 continuous charge/discharge cycles in 1.0 M H_2SO_4 (**a_1**, **a_2** and **a_3**), 1.0 M Na_2SO_4 (**b_1**, **b_2** and **b_3**) and 1.0 M KCl (**c_1**, **c_2** and **c_3**) electrolytes

nanostructure of PPy based electrode in H_2SO_4 electrolyte had no obvious change compared with the morphology after 500 continuous charge/discharge cycles. On the contrary, the nanostructure of PPy based electrodes had slight collapse after 500, 2500 and 5000 continuous charge/discharge cycles in 1.0 M Na_2SO_4 (Fig. 7b_1, b_2 and b_3) and 1.0 M KCl (Fig. 7c_1, c_2 and c_3) electrolytes.

The unique 3D network nanostructure stacked by nanospheres of as-prepared PPy materials collapsed seriously in 1.0 M H_2SO_4 electrolyte during the processes of deoxidation/reoxidation and intercalation/deintercalation of H_3O^+ during the earlier stage of cycling process [52]. Therefore, the collapse of crystal structure or morphology of PPy based electrode might result in the poor cyclic stability in 1.0 M H_2SO_4 electrolyte. The result above was coincident with the conclusion of electrochemical cyclic stability testing.

In order to further investigate the electrochemical performances of as-prepared PPy based electrodes before and after 5000 continuous charge/discharge cycles in 1.0 M H_2SO_4, 1.0 M Na_2SO_4 and 1.0 M KCl electrolytes, EIS measurements were conducted on as-prepared PPy based electrodes in three electrolytes in the frequency range from 10^5 to 10^{-1} Hz (Fig. 8a, b, c). It was shown that the impedance spectra in three electrolytes were composed of a semicircle in the higher frequency region, followed by a linear part in the lower frequency region. Shown in Fig. 8d was an equivalent circuit for fitting the impedance data of as-prepared PPy based electrodes and the corresponding fitting data were listed in Table 2. The intercept of the curves on the real axis was the internal solution resistance (R_s), including bulk electrolyte solution resistance, intrinsic resistance of electroactive materials and contact resistance between current collector and electroactive materials [29].

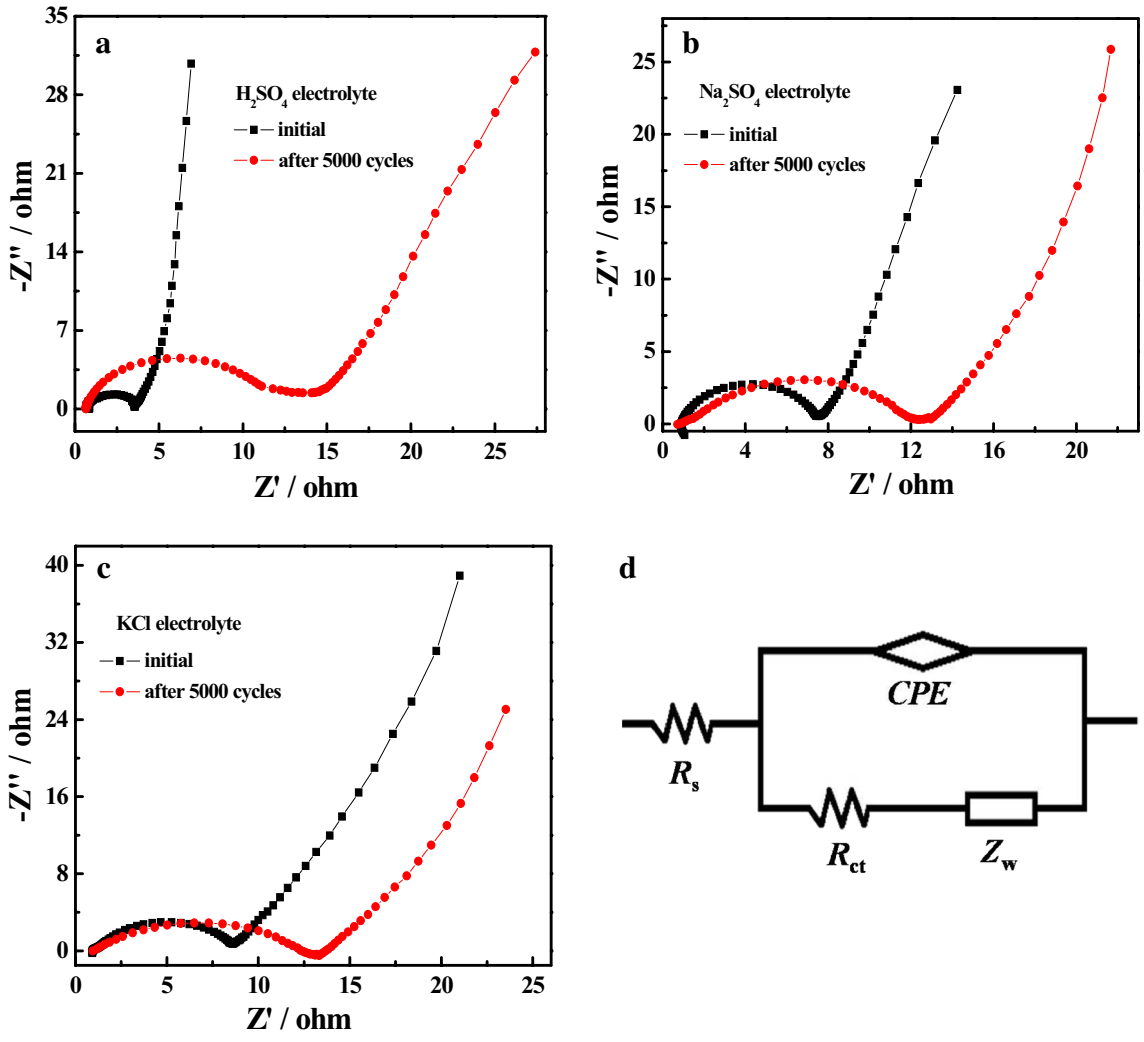

Fig. 8 Nyquist plots of as-prepared PPy based electrodes in 1.0 M H_2SO_4 (**a**), 1.0 M Na_2SO_4 (**b**) and 1.0 M KCl (**c**) electrolytes before and after 5000 continuous charge/discharge cycles, and equivalent circuit for fitting the impedance data of as-prepared PPy based electrodes (**d**)

Table 2 Fitting data of equivalent circuit of impedance spectra of PPy based electrodes before and after 5000 continuous charge/discharge cycles in 1.0 M H_2SO_4, 1.0 M Na_2SO_4 and 1.0 M KCl electrolytes

Electrolytes	1.0 M H_2SO_4	1.0 M Na_2SO_4	1.0 M KCl
After 1st cycle			
R_s (Ω)	2.580	4.383	4.474
Z_w (S-s$^{0.5}$)	0.02537	0.03879	0.03968
R_{ct} (Ω)	2.824	6.299	6.874
CPE (S-s^n)	0.2959	0.3168	0.1490
n[a]	0.8568	0.7710	0.7015
After 5000th cycle			
R_s (Ω)	6.970	6.190	6.650
Z_w (S-s$^{0.5}$)	0.08104	0.07816	0.07785
R_{ct} (Ω)	12.65	11.76	11.95
CPE (S-s^n)	0.3078	0.1874	0.1826
n	0.7563	0.6740	0.6371

[a]Frequency factor

The semicircle in the high frequency region represented the charge transfer resistance (R_{ct}) and the nearly linear plot in the low frequency region stood for the Warburg impedance (Z_w). *CPE* was the constant phase element [53].

It was shown that the semicircle of initial PPy based electrode in 1.0 M H_2SO_4 electrolyte was smaller than that in 1.0 M Na_2SO_4 or 1.0 M KCl electrolyte in the high frequency region, indicating the better change transport in H_2SO_4 electrolyte. The linear slope of initial PPy based electrode in H_2SO_4 electrolyte was more vertical than that in Na_2SO_4 or KCl electrolyte, suggesting that initial PPy based electrode possessed higher conductivity in H_2SO_4 electrolyte. Based on Table 2, it was found that the values of R_s, R_{ct} and Z_w of initial PPy based electrode in H_2SO_4 electrolyte were smaller than those in Na_2SO_4 and KCl electrolytes. The results above indicated that initial PPy based electrode in H_2SO_4 electrolyte exhibited higher capacitive performance than that in Na_2SO_4 or KCl electrolyte.

In addition, due to the collapse of crystal structure or morphology of PPy based electrode in 1.0 M H_2SO_4 electrolyte, the values of R_s, R_{ct} and Z_w after 5000 continuous charge/discharge cycles had a sharp increase compared with those of initial PPy based electrode. It further proved that as-prepared PPy based electrode in 1.0 M H_2SO_4 electrolyte exhibited lower capacitance retention after 5000 continuous charge/discharge cycles. Besides, the values of R_s, R_{ct} and Z_w of as-prepared PPy based electrode in 1.0 M H_2SO_4 electrolyte were similar with those in 1.0 M Na_2SO_4 and 1.0 M KCl electrolytes after 5000 continuous charge/discharge cycles. The results showed that PPy based electrodes possessed similar capacitance performance in three electrolytes after 5000 continuous charge/discharge cycles. These results above were consistent with the tests of CV, GCD and cyclic stability.

4 Conclusions

In summary, CTAB-assisted microemulsion method has been employed to successfully fabricate 3D network nanostructured PPy materials built up by nanospheres with an average diameter of 100 nm. Furthermore, the electrochemical performances of as-prepared PPy based electrode are investigated in 1.0 M H_2SO_4, 1.0 M Na_2SO_4 and 1.0 M KCl electrolytes. It is shown that as-prepared PPy based electrode in 1.0 M H_2SO_4 electrolyte exhibits poorer cyclic stability although the initial specific capacitance is relatively higher than that in 1.0 M Na_2SO_4 or 1.0 M KCl electrolyte. The results in this work adequately illustrate that the 3D nanostructured PPy based electrode exhibits different electrochemical performances in different electrolytes.

Acknowledgements This work was supported by the Longshan academic talent research supporting program of SWUST (18LZX322 and 17LZX406), the National Basic Research Program of China (2014CB846003) and the National Science & Technology Supported Program (2014BAC13B05). Also we are grateful for the help of Analytical and Testing Center of Southwest University of Science and Technology.

References

1. B. Dunn, H. Kamath, J.M. Tarascon, Science **334**, 928–935 (2011)
2. H. Wang, H.B. Feng, J.H. Li, Small **10**, 2165–2181 (2014)
3. M. Mao, S.Z. Chen, P. He, H.L. Zhang, H.T. Liu, J. Mater. Chem. A **2**, 4132–4135 (2014)
4. G.P. Wang, L. Zhang, J.J. Zhang, Chem. Soc. Rev. **41**, 797–828 (2012)
5. C. Largeot, C. Portet, J. Chmiola, P.L. Taberna, Y. Gogotsi, P. Simon, J. Am. Chem. Soc. **130**, 2730–2731 (2008)
6. X. Li, Y. Tang, J.H. Song, W. Yang, M.S. Wang, C.Z. Zhu, W.G. Zhao, J.M. Zheng, Y.H. Lin, Carbon **129**, 236–244 (2018)
7. Y.H. Wang, P. He, W. Lei, F.Q. Dong, T.H. Zhang, Compos. Sci. Technol. **103**, 16–21 (2014)
8. W.F. Wei, X.W. Cui, W.X. Chen, D.G. Ivey, Chem. Soc. Rev. **40**, 1697–1721 (2011)
9. J. Yan, Q. Wang, T. Wei, Z.J. Fan, Adv. Energy Mater. **4**, 157–164 (2014)
10. M. Yu, J. Li, L.J. Wang, Chem. Eng. J. **310**, 300–306 (2017)
11. S.L. Candelaria, Y.Y. Shao, W. Zhou, X.L. Li, J. Xiao, J.G. Zhang, Y. Wang, J. Liu, J.H. Li, G.Z. Cao, Nano Energy **1**, 195–220 (2012)
12. X. Zhang, J.M. Wang, J. Liu, J. Wu, H. Chen, H. Bi, Carbon **115**, 134–146 (2017)
13. X.H. Xia, Y.Q. Zhang, D.L. Chao, C. Guan, Y.J. Zhang, L. Li, X. Ge, I.M. Bacho, J.P. Tu, H.J. Fan, Nanoscale **6**, 5008–5048 (2014)
14. Y. Wang, H. Dou, J. Wang, B. Ding, Y.L. Xu, Z. Chang, X.D. Hao, J. Power Source **327**, 221–228 (2016)
15. X.Y. Yu, L. Yu, X.W. Lou, Adv. Energy Mater. **6**, 1501333 (2016)
16. Q.F. Meng, K.F. Cai, Y.X. Chen, L.D. Chen, Nano Energy **36**, 268–285 (2017)

17. A. Eftekhari, L. Li, Y. Yang, J. Power Sources **347**, 86–107 (2017)
18. F.H. Hsu, T.M. Wu, J. Mater. Sci.-Mater. Electron. **29**, 382–391 (2018)
19. G.A. Snook, P. Kao, A.S. Best, J. Power Sources **196**, 1–12 (2011)
20. Z.G. Yin, Q.D. Zheng, Adv. Energy Mater. **2**, 179–218 (2012)
21. A. Singh, A. Chandra, J. Appl. Electrochem. **43**, 773–782 (2013)
22. W. Sun, R.L. Zheng, X.Y. Chen, J. Power Sources **195**, 7120–7125 (2010)
23. R.S. Salunke, C.K. Kasar, M.A. Bangar, P.G. Chavan, D.J. Shirale, J. Mater. Sci.-Mater. Electron. **28**, 14672–14677 (2017)
24. M. Merisalu, T. Kahro, J. Kozlova, A. Niilisk, A. Nikolajev, M. Marandi, A. Floren, H. Alles, V. Sammelselg, Synth. Met. **200**, 16–23 (2015)
25. J.H. Huang, Z.H. Yang, B. Yang, R.J. Wang, T.T. Wang, J. Power Sources **271**, 143–151 (2014)
26. S. Peshoria, A.K. Narula, J. Mater. Sci.-Mater. Electron. **28**, 18348–18356 (2017)
27. Z.N. Yu, L. Tetard, L. Zhai, J. Thomas, Energy Environ. Sci. **8**, 702–730 (2015)
28. X.T. Zhang, J. Zhang, W.H. Song, Z.F. Liu, J. Phys. Chem. B **110**, 1158–1165 (2006)
29. Q.F. Wu, K.X. He, H.Y. Mi, X.G. Zhang, Mater. Chem. Phys. **101**, 367–371 (2007)
30. Y.J. Song, R.M. Garcia, R.M. Dorin, H.R. Wang, Y. Qiu, E.N. Coker, W.A. Steen, J.E. Miller, J.A. Shelnut, Nano Lett. **7**, 3650–3655 (2007)
31. R. Temmer, I. Must, F. Kaasik, A. Aabloo, T. Tamm, Sens Actuator B **166–167**, 411–418 (2012)
32. B. Wei, L.D. Wang, Q.H. Miao, Y.N. Yuan, P. Dong, R. Vajtai, W.D. Fei, Carbon **85**, 249–260 (2015)
33. A.K. Ganguli, A. Ganguly, S. Vaidya, Chem. Soc. Rev. **39**, 474–485 (2010)
34. C. Aubery, C. Solans, S. Prevost, M. Gradzielski, M. Sanchez-dominguez, Langmuir **29**, 1779–1789 (2013)
35. C. Zhong, Y.D. Deng, W.B. Hu, J.L. Qian, L. Zhang, J.J. Zhang, Chem. Soc. Rev. **44**, 484–539 (2015)
36. A. González, E. Goikolea, J.A. Barrena, R. Mysyk, Renew. Sust. Energ. Rev. **58**, 1189–1206 (2016)
37. M. Mirzaeian, Q. Abbas, A. Ogwu, P. Hallb, M. Goldinc, M. Mirzaeiand, H.F. Jirandehid, Int. J. Hydrogen Energy **42**, 25565–25587 (2017)
38. M. Li, L.L. Yang, J. Mater. Sci.-Mater. Eletron. **26**, 747–754 (2015)
39. Y. Xia, J. Yang, Synth. Met. **160**, 1688–1691 (2010)
40. W. Lei, P. He, Y.H. Wang, S.S. Zhang, F.Q. Dong, H.T. Liu, Electrochim. Acta **132**, 112–117 (2014)
41. S.P. Palaniappan, P. Manisankar, Mater. Chem. Phys. **122**, 15–17 (2010)
42. P.M. Kulal, D.P. Dubal, C.D. Lokhande, V.J. Fulari, J. Alloy. Compd. **509**, 2567–2571 (2011)
43. Y. Huang, H.F. Li, Z.F. Wang, M.S. Zhu, Z.X. Pei, Q. Xue, Y. Huang, C.Y. Zhi, Nano Energy **22**, 422–438 (2016)
44. A. Osterholm, T. Lindfors, J. Kauppila, P. Damlin, C. Kvarnstrom, Electrochim. Acta **83**, 463–470 (2012)
45. H.Y. Mi, X.G. Zhang, X.G. Ye, S.D. Yang, J. Power Sources **176**, 403–409 (2008)
46. M. Rajesh, C.J. Raj, B.C. Kim, B. Cho, J.M. Ko, K.H. Yu, Electrochim. Acta **220**, 373–383 (2016)
47. F. Wolfart, D.P. Dubal, M. Vidotti, R. Holze, P. Gómez-Romero, J. Solid State Electrochem. **20**, 901–910 (2016)
48. H.J. Yu, J.H. Wu, L.Q. Fan, Y.Z. Lin, K.Q. Xu, Z.Y. Tang, C.X. Cheng, S. Tang, J.M. Lin, M.L. Huang, Z. Lan, J. Power Sources **198**, 402–407 (2012)
49. A. Afzal, F.A. Abuilaiwi, A. Habib, M. Awais, J. Power Sources **362**, 174–186 (2017)
50. S. Paul, K.S. Choi, J.L. Dong, P. Sudhagar, Y.S. Kang, Electrochim. Acta **78**, 649–655 (2012)
51. J.K. Lee, H. Jeong, R. Lavall, A. Busnaina, Y.L. Kim, Y.J. Jung, H.Y. Lee, ACS Appl. Mater. Interfaces **9**, 33203–33211 (2017)
52. W. Lei, P. He, S.S. Zhang, F.Q. Dong, Y.J. Ma, J. Power Sources **266**, 347–352 (2014)
53. J.W. Lee, T. Ahn, D. Soundararajan, J.M. Ko, J.D. Kim, Chem. Commun. **47**, 6305–6307 (2011)